Available online at www.sciencedirect.com
ScienceDirect
Trans. Nonferrous Met. Soc. China 31(2021) 3772−3784
Transactions of Nonferrous Metals Society of China
www.tnmsc.cn

# Effect of elevated-temperature annealing on microstructure and properties of Cu−0.15Zr alloy

Zi-chen ZHANG[1], Ri-chu WANG[1,2], Chao-qun PENG[1],
Yan FENG[1,2], Xiao-feng WANG[1,2], Xiang WU[3], Zhi-yong CAI[1,2]

1. School of Materials Science and Engineering, Central South University, Changsha 410083, China;
2. Hunan Province Key Laboratory of Electronic Packaging and Advanced Functional Materials, Central South University, Changsha 410083, China;
3. College of Materials Science and Engineering, Changsha University of Science and Technology, Changsha 410114, China

Received 7 December 2020; accepted 8 September 2021

**Abstract:** Cu−0.15Zr (wt.%) alloy with uniform and fine microstructure was fabricated by rapid solidification followed by hot forging. Evolution of microstructure, mechanical properties and electrical conductivity of the alloy during elevated-temperature annealing were investigated. The alloy exhibits good thermal stability, and its strength decreases slightly even after annealing at 700 °C for 2 h. The nano-sized $Cu_5Zr$ precipitates show significant pinning effect on dislocation moving, which is the main reason for the high strength of the alloy. Additionally, the large-size $Cu_5Zr$ precipitates play a major role in retarding grain growth by pinning the grain boundaries during annealing. After annealing at 700 °C for 2 h, the electrical conductivity of samples reaches the peak value of 88% (IACS), which is attributed to the decrease of vacancy defects, dislocations, grain boundaries and Zr solutes.

**Key words:** Cu−Zr alloy; rapid solidification; annealing; microstructure; tensile strength; electrical conductivity

## 1 Introduction

Cu alloys with superior electrical and thermal conductivities, high strength, and good ductility show great prospect in lead frame for integrated circuit, railway contact wire, electronic connectors, and thrust chamber of rocket engines [1−5]. Generally, the above-mentioned Cu alloys are designed with the addition of small amounts of alloying elements, e.g. Cr, Nb, Ag, and Zr, to enhance the strength. These alloying elements have a low solid solubility at room temperature and exhibit minor adverse effect on electrical conductivity. It is reported that the addition of Zr is beneficial to improving the tensile strength and thermal stability of Cu alloy [6]. Cu−Zr alloy is one of the materials with high conductivities, good strength and excellent ductility at elevated temperature, which has attracted considerable interest in the recent years [7,8].

It is known that $Cu_5Zr$ phase exhibits good thermal stability at high temperature, and plays a crucial role in strengthening the Cu−Zr alloy [8]. PENG et al [9] confirmed that the aging sequence of the Cu−0.12Zr alloy is supersaturated solid solution, Zr-rich atomic clusters, followed by semi-coherent $Cu_5Zr$ phase. NAKASHIMA et al [8] demonstrated that the $Cu_5Zr$ phase in the Cu−0.13Zr alloy presents two different morphologies during aging: spherical particles and disk-shaped particles, respectively. After aging treatment, the

**Corresponding author:** Zhi-yong CAI, Tel: +86-731-88836638, E-mail: zycaimse@163.com
DOI: 10.1016/S1003-6326(21)65763-1

depletion of Zr solute atoms in the matrix is beneficial to improving electrical conductivity, while a large number of $Cu_5Zr$ precipitates contribute to the excellent strength [1,10].

To decrease the burning loss of Zr element during high temperature melting, Cu−Zr alloy is usually prepared by vacuum melting and casting, followed by solution treatment and plastic deformation [11,12]. However, the maximum equilibrium solid solubility of Zr in Cu is only approximately 0.12 at.% at 972 °C. The low solidification rate of traditional casting process will lead to serious macro-segregation in Cu−Zr alloy [7,13,14]. The large-sized Zr-rich phase cannot be dissolved by solid solution treatment or crushed by plastic deformation. Therefore, the properties of the Cu−Zr alloy are highly restricted [15]. Fortunately, a high-strength alloy with fine and uniform microstructure can be obtained by rapid solidification/powder metallurgy route due to the high solidification rate during atomization process [16,17]. Gas atomization has a high degree of supercooling, resulting in the formation of metastable solid solution of the alloy elements with low solubility in Cu [18−20]. Additionally, rapid solidification also contributes to obtaining finer grains and precipitates as compared with the casting method [21]. Such a fine microstructure is helpful for improving the strength and plasticity of the alloy simultaneously [22].

In this work, Cu−0.15Zr alloy reinforced by fine and uniformly distributed second-phase particles was prepared by gas atomization followed by hot isostatic pressing (HIP) and forging. In consideration of the high-temperature service environment when used as thrust chamber material for rocket engines, the microstructural evolution, electrical conductivity and mechanical properties of the alloy after elevated-temperature annealing were investigated.

## 2 Experimental

The raw materials were electrolytic Cu (99.99% in purity) and Cu−50%Zr master alloy. The pre-alloyed Cu−0.15Zr powder was prepared by vacuum melting and gas atomization under argon atmosphere. Metallic Cu and Cu−50%Zr master alloy were placed into crucible, and then the atomizing chamber was completely sealed and vacuumed. After the vacuum reached $1.0\times10^{-2}$ Pa, argon gas was fed into the chamber till it went back to normal atmospheric pressure. The melting crucible was then heated, and the temperature was adjusted to 1350 °C for 30 min after the alloy was completely melted. During atomization, the molten Cu−0.15Zr alloy was poured into a pre-heated tundish and impacted by a high argon gas at 1.2 MPa to obtain the pre-alloyed powder. Detailed chemical composition of the as-atomized powder is given in Table 1. The pre-alloyed powder was mechanically sieved through 200 mesh (less than 74 μm), and then filled into a cylindrical steel can with an inner size of *d*120 mm × 180 mm. Tap density of the powder was approximately 5.3 g/cm$^3$. The can filled with powder was vacuum degassed at room temperature for 2 h, and then degassed at 400 °C for 2 h. The sealed can reached the vacuum level of $1\times10^{-3}$ Pa. The pre-alloyed powder was densified by hot isostatic pressing (HIP) at 830 °C and 150 MPa for 2 h, followed by forging.

**Table 1** Chemical composition of pre-alloyed powder (wt.%)

| Zr | Cr | Al | Ni | |
|---|---|---|---|---|
| 0.1475 | 0.0704 | 0.0050 | 0.0047 | |
| Fe | Mg | Ag | O | Cu |
| 0.0034 | 0.0015 | 0.0013 | 0.0029 | Bal. |

Chemical composition of the pre-alloyed powder was analyzed using an inductively coupled plasma optical emission spectrometer (ICP-OES, SPECTRO BLUE SOP, Germany). Microstructures were observed with optical microscope (OM, Leica DMI 300M, Germany), scanning electron microscope (SEM, Quanta 200, Holland) equipped with electron backscatter diffraction (EBSD) system, and transmission electron microscope (TEM, Titan G2 60-300, America) equipped with an energy dispersive X-ray spectrometer (EDS). The samples for OM and SEM observations were mechanically polished using conventional method, and the OM samples were etched by 5 g $FeCl_3$ + 20 mL HCl + 100 mL $H_2O$ solution. The samples for TEM and EBSD observations were twin-jet electro-polished using a solution of 60 vol.% $CH_3OH$ and 40 vol.% $HNO_3$ at about −30 °C and 10−16 V. Electrical resistivity of the samples was measured by a double arm electrical bridge device

(QJ36S, China). Tensile tests were performed at room temperature with a constant strain rate of 2 mm/min on a test machine (MTS 810, America). The samples of tensile tests are rod-shaped, with a deformation area of 50 mm in length and 9 mm in diameter. Three samples were tested under each condition. The tensile fractured surfaces of the samples were observed by SEM.

## 3 Results and discussion

### 3.1 Microstructural characteristics

Optical microstructures of HIPed Cu−0.15Zr alloy at different states are presented in Fig. 1. It is seen from Fig. 1(a) that fine and equiaxed grains with a maximum size of only 6 μm are observed.

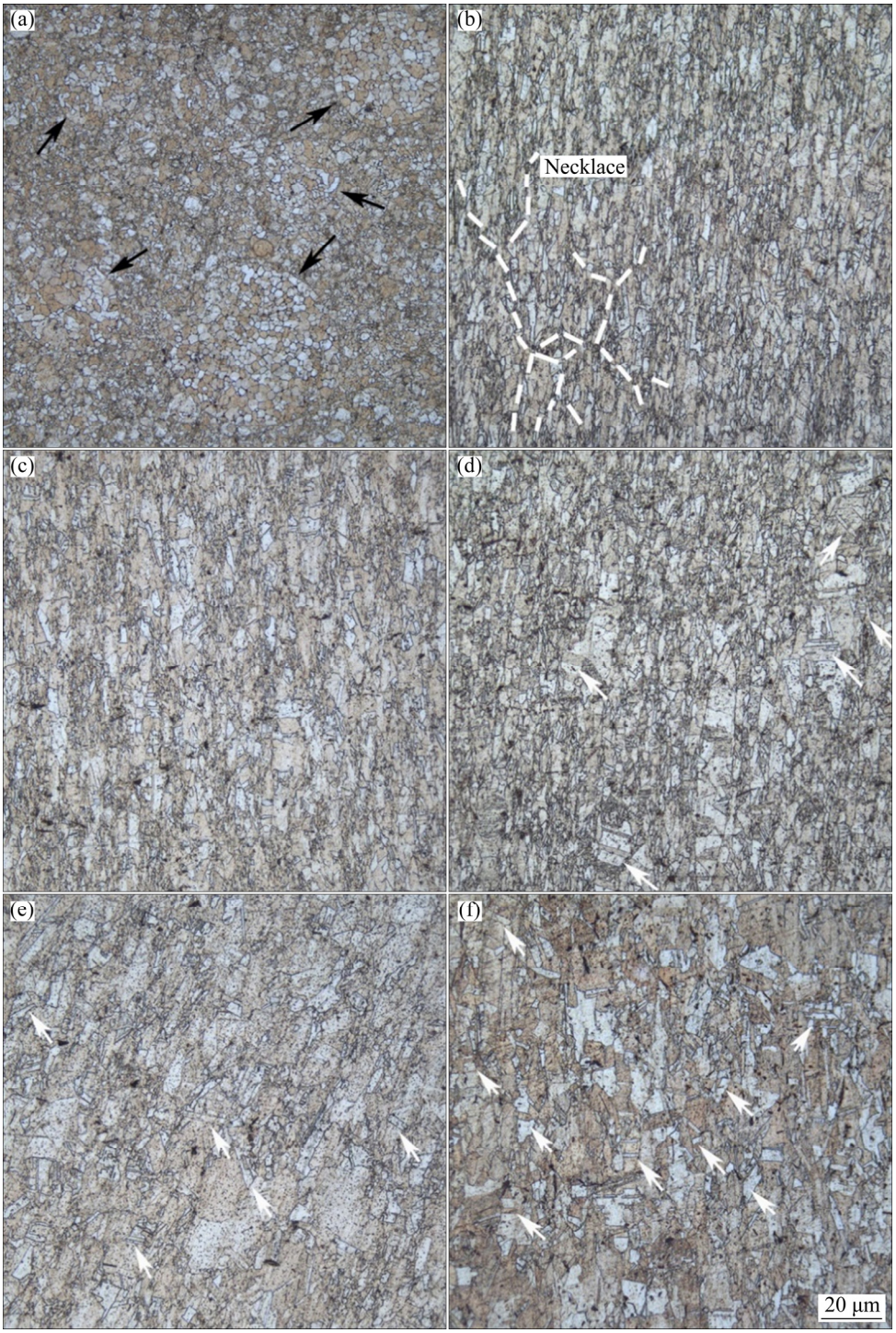


**Fig. 1** Optical microstructures of HIPed alloy (a), forged alloy (b), and annealed alloy at 600 (c), 700 (d), 800 (e) and 900 °C (f)

However, the prior particle boundaries (PPBs) of spherical-shaped powder are quite evident, as indicated by the arrows. It is known that the presence of PPBs will lead to the formation of microvoids and cracks, resulting in poor ductility [23,24]. The PPBs are broken and formed tightly during the forging process, and the microstructure uniformity is improved (Fig. 1(b)). The primary equiaxed grains are elongated and a large number of ultrafine grains with necklace structure appear around the elongated grains. This phenomenon indicates that dynamic recrystallization occurs during forging of the HIPed alloy. After the forged alloy was annealed at 600 °C for 2 h, the number of recrystallized grains decreases slightly, and some annealing twins appear in the larger size grains (as pointed by the white arrows). As shown in Figs. 1(e, f), when the annealing temperature is increased to 800 °C and above, the grains in the alloy are obviously coarsened and the thickness of twin lamella increases with grain boundary (GB) migration.

Figures 2 and 3 display the SEM images of the forged Cu−0.15Zr alloy before and after annealing at various temperatures. As shown in Fig. 2(a), particles larger than 200 nm are clearly observed at the GBs and within grains of the as-forged alloy. Additionally, nano-sized continuous precipitates dispersed in the matrix can be observed in the high magnification image (Fig. 2(b)). After annealing at 600 ° for 2 h, there is no significant change in the volume fraction and size of the large size particles and the continuous precipitates, as seen in Figs. 2(c, d). However, it can also be seen that some nano-sized particles precipitate at the GBs (indicated by green circles). It is known that the GB segregation or GB precipitation is more likely to occur during heat treatment, because the GB

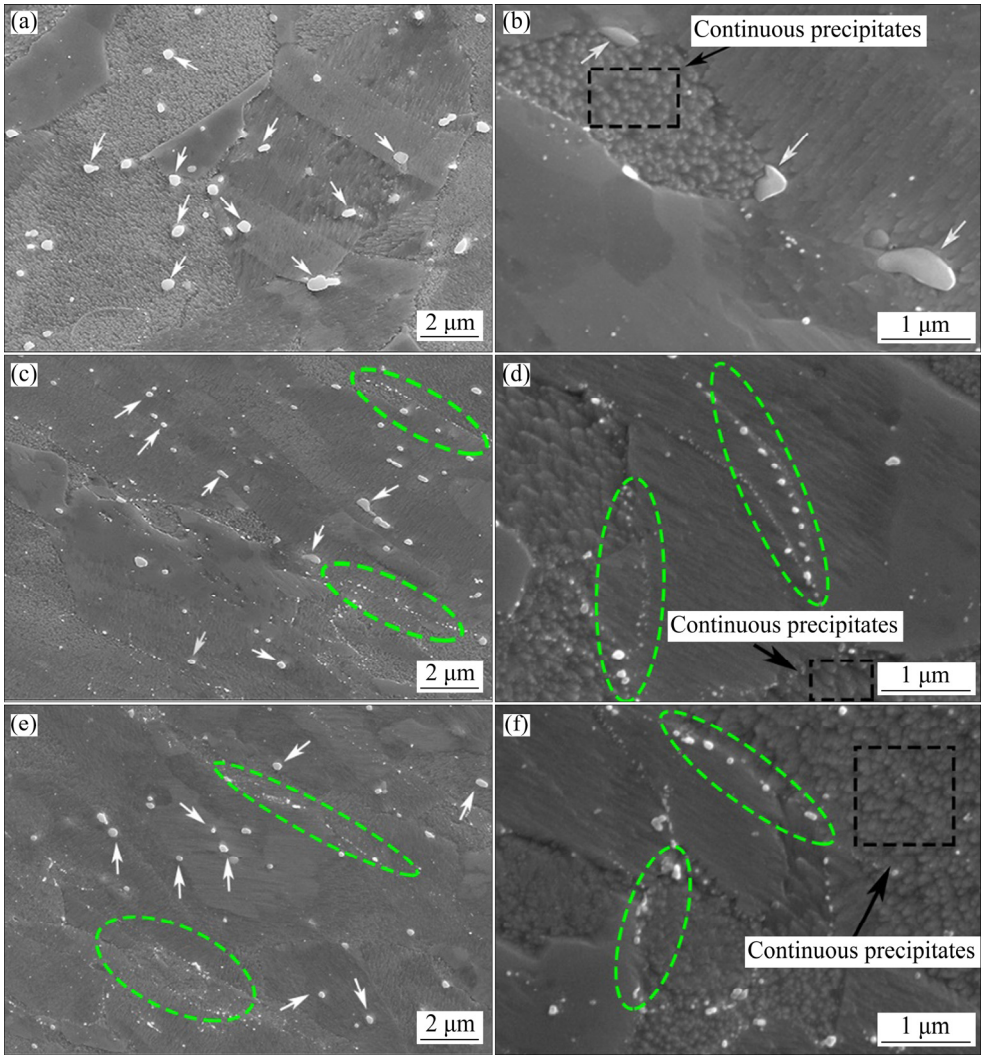


**Fig. 2** SEM microstructures of Cu−0.15Zr alloy after forging (a, b) and annealing at 600 (c, d) and 700 °C (e, f) for 2 h

diffusion is reasonably higher than the bulk diffusion. Compared with the alloy annealed at 600 °C, the volume fraction and size of large size particles in the matrix annealed at 700 °C are noticeably smaller, and more nano-sized GB precipitates are observed (Figs. 2(e, f)). With further increasing the annealing temperature, the volume fraction of the large size particles decreases gradually, due to the accelerated diffusion along GBs. When the sample is exposed at 900 °C for 2 h, these large size particles are completely dissolved, while the number of nano-sized precipitates at the GBs increases obviously. Based on the above results, the volume fraction and size of large size particles are all very stable when the forged Cu−0.15Zr alloy is annealed below 700 °C. At the same time, the number of the nano-sized GB precipitates increases gradually with the dissolution of large size particles. It can also be noted in Figs. 3(b, d) that the continuous precipitates in the matrix are extremely stable even during high temperature annealing.

The large size particles, nano-sized GB precipitates and continuous precipitates in the matrix were further investigated by TEM, and the bright field TEM images of the forged alloy are displayed in Fig. 4. It can be seen that particles larger than 200 nm are formed in the matrix. EDS results (Fig. 5) of these particles illustrate that the atomic ratio of Cu to Zr in the large size particles is approximately 5:1, which is in consistent with the $Cu_5Zr$ phase reported [14,25,26]. These $Cu_5Zr$ particles play a role in accumulating dislocations during forging of the alloy.

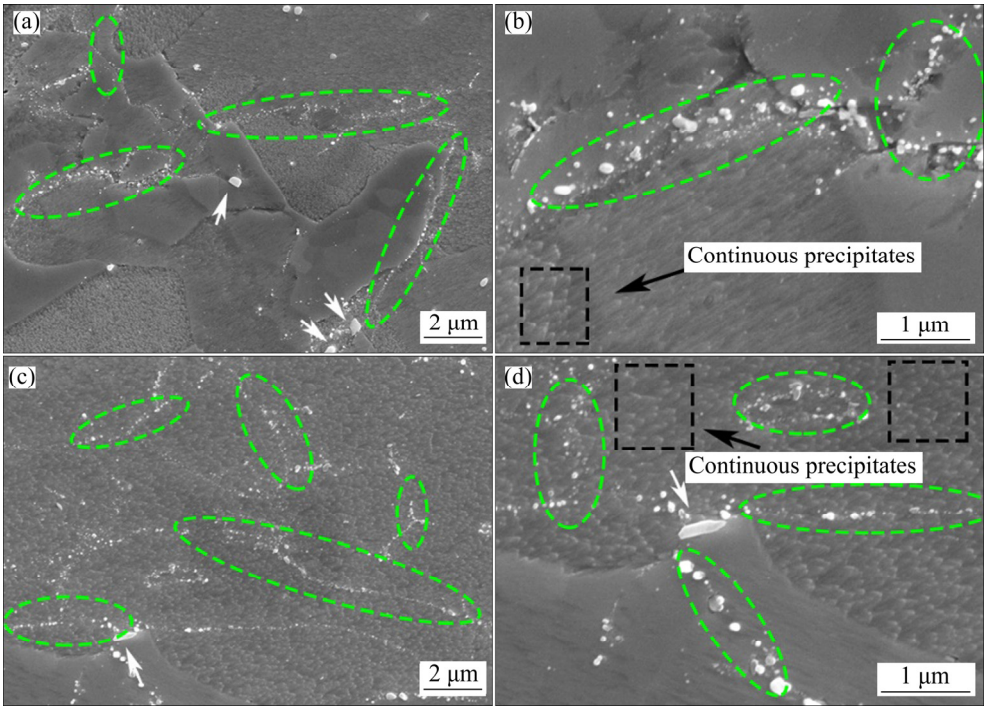


**Fig. 3** SEM microstructures of Cu−0.15Zr alloy after annealing at 800 (a, b) and 900 °C (c, d) for 2 h

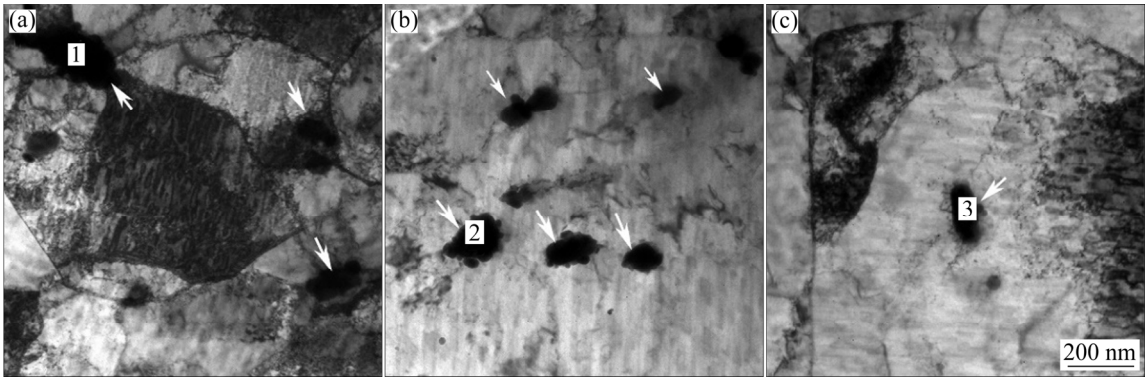


**Fig. 4** TEM microstructures of $Cu_5Zr$ precipitates in forged alloy

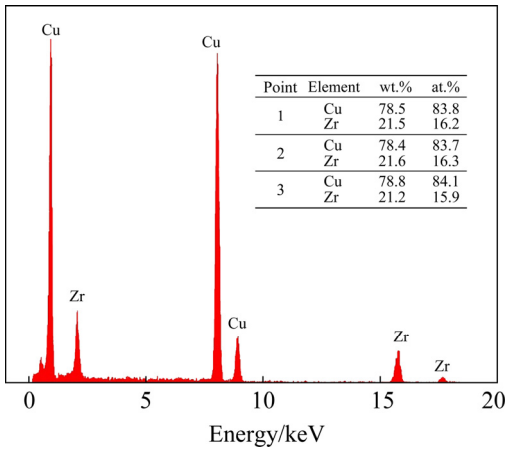


**Fig. 5** EDS result of $Cu_5Zr$ precipitates marked in Fig. 4

Figure 6(a) presents the bright field TEM images of nano-sized GB precipitates in the alloy after annealing at 600 °C for 2 h. It can be seen that the discontinuous GB precipitates with size less than 100 nm are nearly spherical. Compared with Fig. 3, after annealing at 800 °C and above, the number of nano-sized GB precipitates in the sample increases remarkably. With the increase of temperature, the diffusion rate of Zr atom increases, and some large size $Cu_5Zr$ particles gradually dissolve, providing more diffusible Zr atoms in the matrix. It is known that the GBs are the fast diffusion paths of solute atoms, and also the places where the preferential nucleation of precipitates occurs at high temperatures. GB segregation can decrease the driving force of grain coarsening by reducing the conventional high-angle GB energy [27,28]. Figure 6(c) shows the twins of the alloy annealed at 800 °C for 2 h, and the thickness of the twin lamella is approximately 2 μm.

A large number of continuous precipitates smaller than 10 nm are observed in the forged alloy (Fig. 7(a)), and dislocations are trapped and accumulated around these fine precipitates. According to the selected area electron diffraction (SAED) pattern (Fig. 7(b)) and the corresponding schematic analysis (Fig. 7(c)), these continuous precipitates in the matrix are $Cu_5Zr$ phases, which are coherent with the Cu matrix. These results are in consistent with those in literatures [8,9,29]. Figures 8(a, d**)** illustrate the evolution of nano-sized $Cu_5Zr$ precipitates annealed at different temperatures. According to the statistics analysis in Figs. 8(e), the average size of $Cu_5Zr$ precipitates increases slightly with the increase of annealing temperature. The dislocation density in the annealed alloy decreases, while the volume fraction of $Cu_5Zr$ precipitates increases slightly. Moreover, only a few "bean-like" precipitates become relatively coarse when the annealing temperature exceeds 700 °C, as indicated by arrows, suggesting that the coherence between the precipitates and the matrix is broken at high temperatures [30−32]. It can be concluded that in the high-temperature annealing process below 700 °C, the continuous precipitates in the matrix are very stable, and the fine and stable $Cu_5Zr$ precipitates can trap and accumulate dislocations to provide obvious strain hardening during tensile test.

Inverse pole maps of the samples before and after annealing are shown in Fig. 9. High angle grain boundaries (HAGBs, misorientation >15°) are plotted as black lines, while low angle grain boundaries (LAGBs, misorientation <15°) are plotted as white lines. The corresponding misorientation angle distributions are presented in Fig. 10. Microstructure of the forged Cu−0.15Zr alloy is characterized by fine/equiaxed grains and

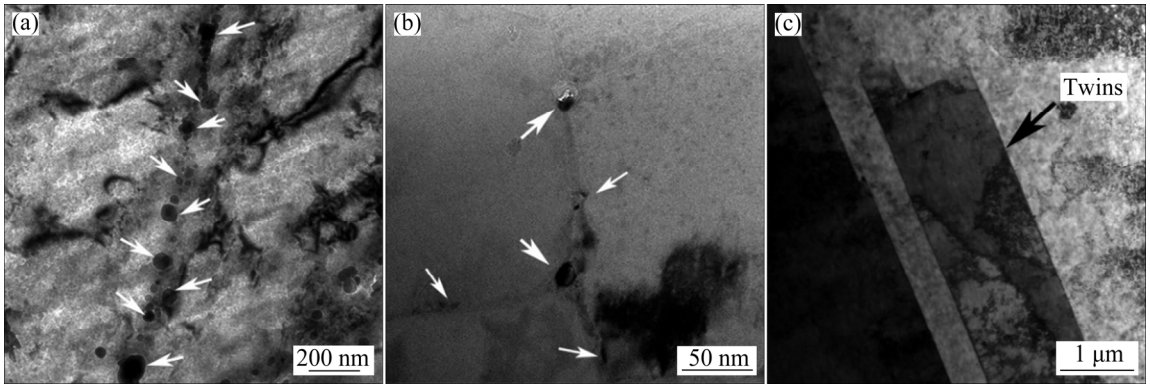


**Fig. 6** TEM morphologies of discontinuous precipitates at GBs in alloy annealed at 600 °C (a, b), and twins in alloy annealed at 800 °C (c)

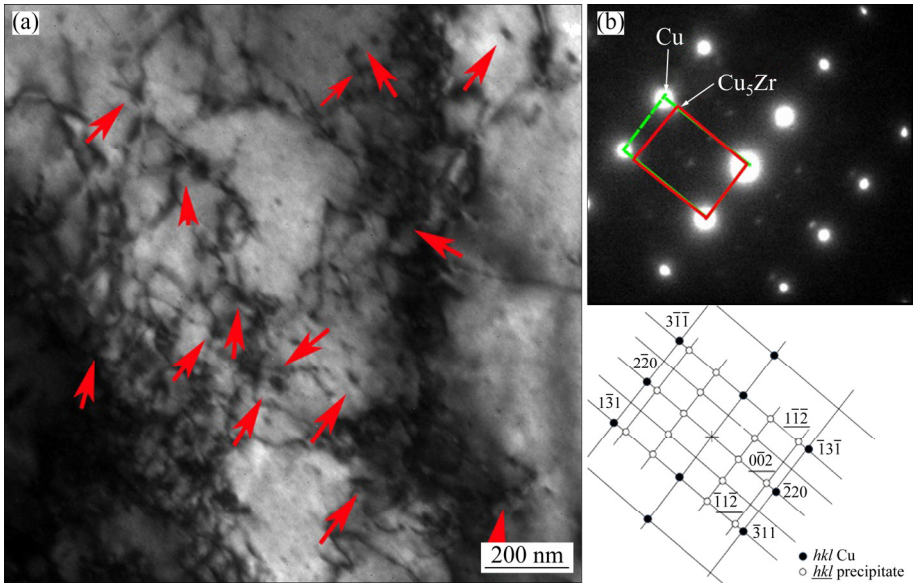


**Fig. 7** TEM microstructure of $Cu_5Zr$ precipitates and dislocations in forged alloy (a) and SAED pattern (b) (The electron beam is parallel to $[112]_{Cu}$)

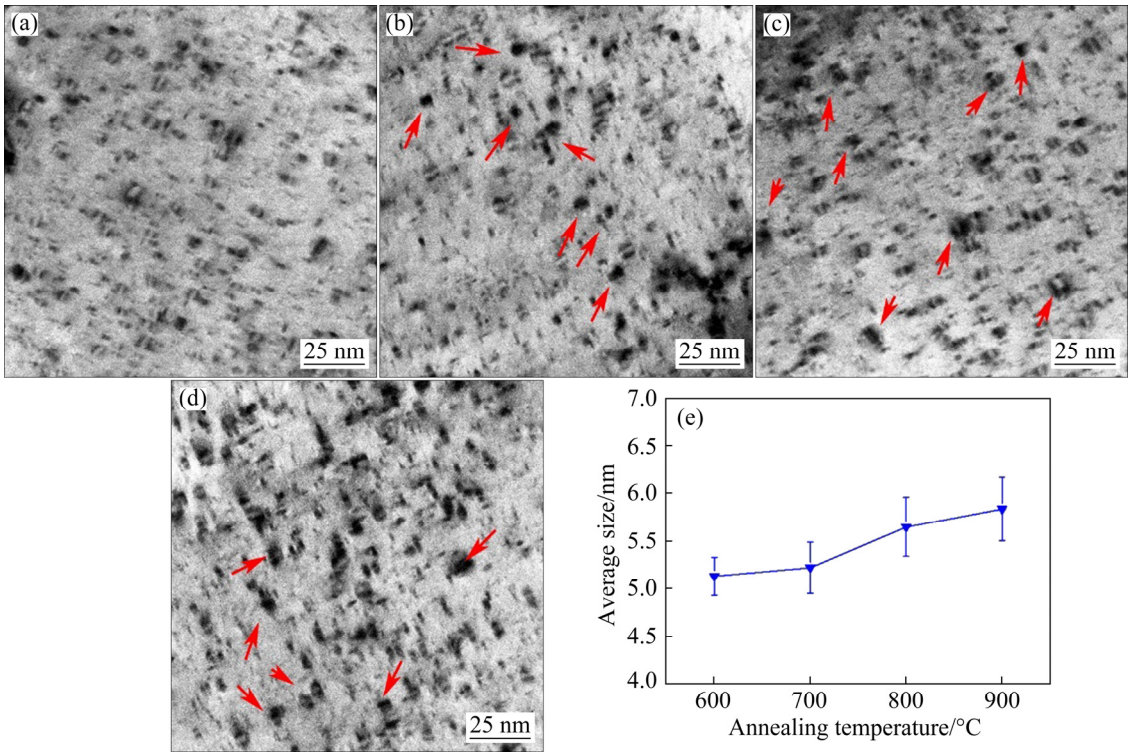


**Fig. 8** TEM microstructures of nano-sized $Cu_5Zr$ precipitates in matrix of alloy annealed at 600 (a), 700 (b), 800 (c) and 900 °C (d) for 2 h, and variation of average size for nano-sized $Cu_5Zr$ with annealing temperature (e)

large/elongated grains, indicating that partial dynamic recrystallization occurs in the alloy. Additionally, some LAGBs are observed in the large/elongated grains, and 31% of the boundaries are calculated to be LAGBs. After annealing at 700 °C for 2 h, the number of fine/equiaxed grains decreases slightly, and the number fraction of LAGBs reduces to 17%. It is found that after annealing at 800 °C, only a small number of fine/equiaxed grains are observed, and the number fraction of LAGBs decreases to 9%. Generally, the LAGBs are mainly associated with the dislocations and dislocation cells, which means that the lower number fraction of LAGBs is consistent with the lower density of dislocations in the alloy [33]. When the annealing temperature rises to 900 °C, the

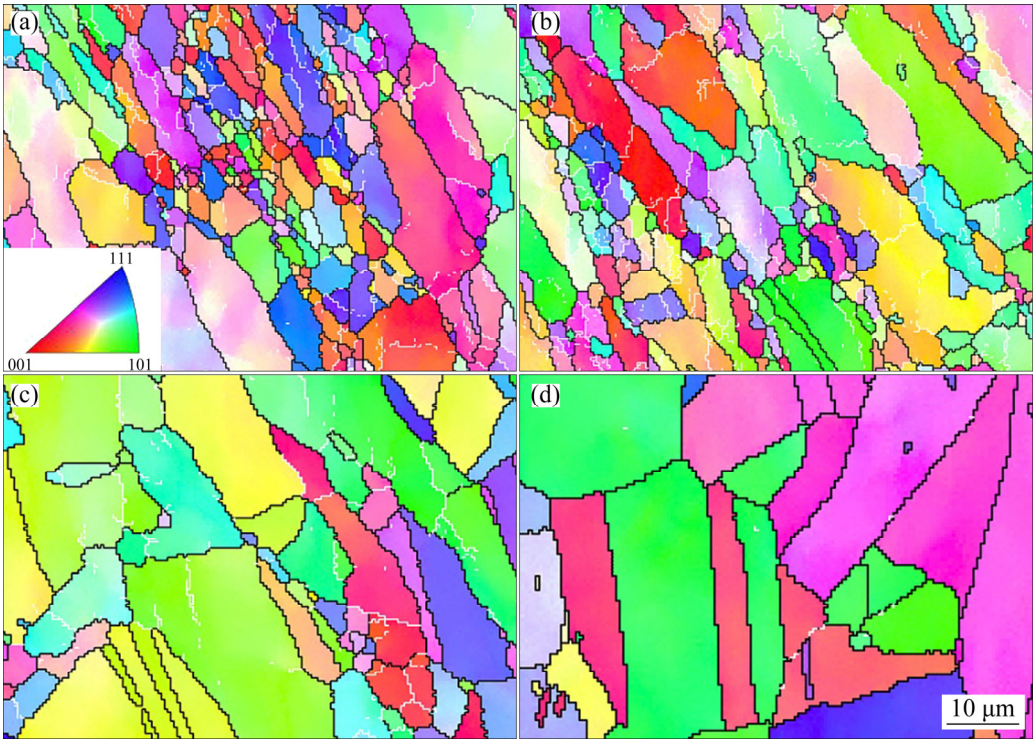


**Fig. 9** EBSD orientation maps of alloy after forging (a) and annealing at 700 (b), 800 (c) and 900 °C (d) for 2 h (The inserted color code is used to identify the crystallographic orientations)

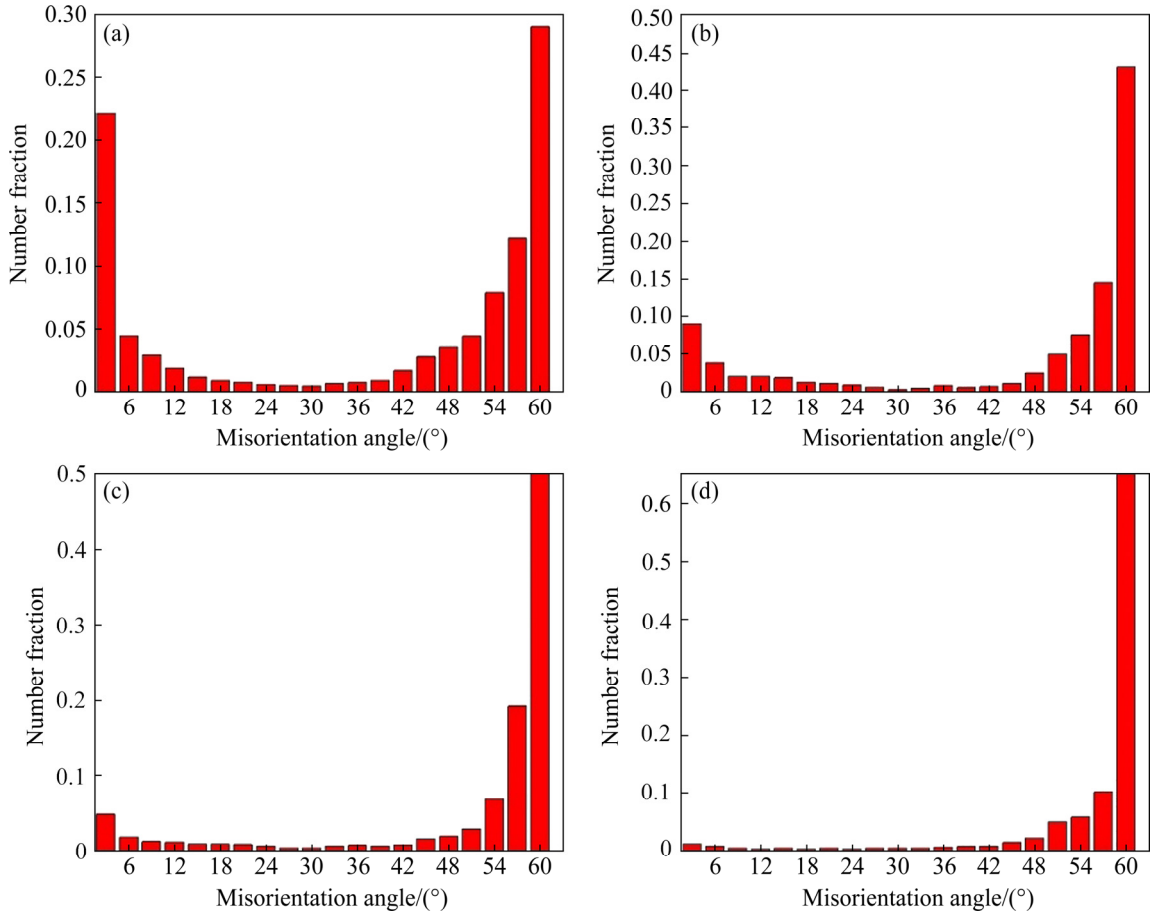


**Fig. 10** Misorientation angle distributions of alloy after forging (a) and annealing at 700 (b), 800 (c) and 900 °C (d) for 2 h

fine/equiaxed grains are completely consumed and almost all LAGBs transform into straight and flat HAGBs by absorbing dislocations during annealing.

The variation of average grain size of the forged alloy with annealing temperature is plotted in Fig. 11. The grain size information is obtained from the EBSD orientation map and OM image. The average grain size of the forged alloy measured by EBSD is 9.5 μm, which is smaller than that the result determined by OM image of 13.5 μm. It is known that the visibility of GBs under optical microscopy is related to the boundary state, such as precipitation distribution, solute content around the GBs and misorientation angle [34]. However, these factors have little influence on the identification of GBs by EBSD method. Moreover, some small grains are lost even if the alloy is etched due to the relatively lower resolution level of optical micrograph. This means that the statistical grain size from EBSD is more accurate. After annealing at 700 °C for 2 h, the grain size of forged alloy increases slightly, and the average grain size obtained by EBSD is approximately 12.3 μm. The GB migration velocity is accelerated with the increase of temperature. As depicted in Fig. 2(e), even after annealing at 700 °C for 2 h, a considerable number of large size granular $Cu_5Zr$ particles are retained in the alloy. This plays a vital role in preventing grain growth by pinning the migration of GBs at high temperature. When the annealing temperature is 800 °C, the number and size of large size granular $Cu_5Zr$ particles decrease significantly, and the average grain size increases to 19.2 μm according to the EBSD data. The chain-like precipitates at the GBs and the nano-size $Cu_5Zr$ precipitates in the matrix are too small to pin the GB, and the large size granular $Cu_5Zr$ particles are dissolved, so the grain growth rate increases rapidly. As the annealing temperature increases to 900 °C, the average grain size analyzed by EBSD is approximately 22.0 μm.

### 3.2 Mechanical properties

Figure 12 shows the variation of tensile properties of the alloy with the annealing temperature. The yield strength (YS), ultimate tensile strength (UTS) and elongation of the forged alloy are 164 MPa, 289 MPa and 40%, respectively. With the increase of annealing temperature, the YS and UTS of the alloy decrease, but the elongation increases. When the annealing temperature is not higher than 750 °C, the UTS and YS drop slightly. The large size granular $Cu_5Zr$ precipitates effectively slow down the grain growth rate. When the annealing temperature rises to 800 °C, the fraction of LAGBs, large size granular $Cu_5Zr$ particles and fine/equiaxed grains decreases sharply, and the strength of annealed sample decreases most. After the alloy was exposed at 900 °C for 2 h, the large size granular $Cu_5Zr$ particles are almost completely dissolved, and the number of GB precipitates increases significantly. Discontinuous GB precipitates have weak pinning effect on GBs, resulting in the lowest UTS and YS of 92 MPa and 246 MPa, respectively.

The fracture surfaces of the samples after tensile tests were observed by SEM, and the results are shown in Fig. 13. It can be seen that the fracture surfaces of all samples are cup-shaped and cone-

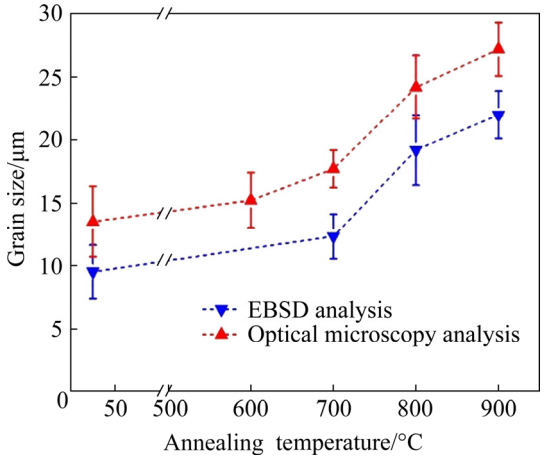


**Fig. 11** Influence of annealing temperature on grain size of rapidly solidified and forged Cu−0.15Zr alloy

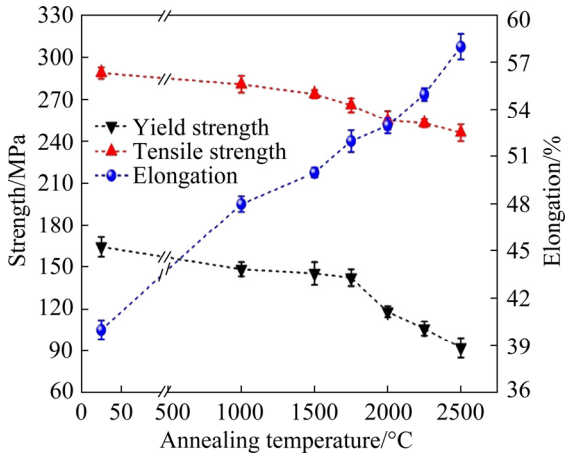


**Fig. 12** Influence of annealing temperature on tensile properties of Cu−0.15Zr alloy

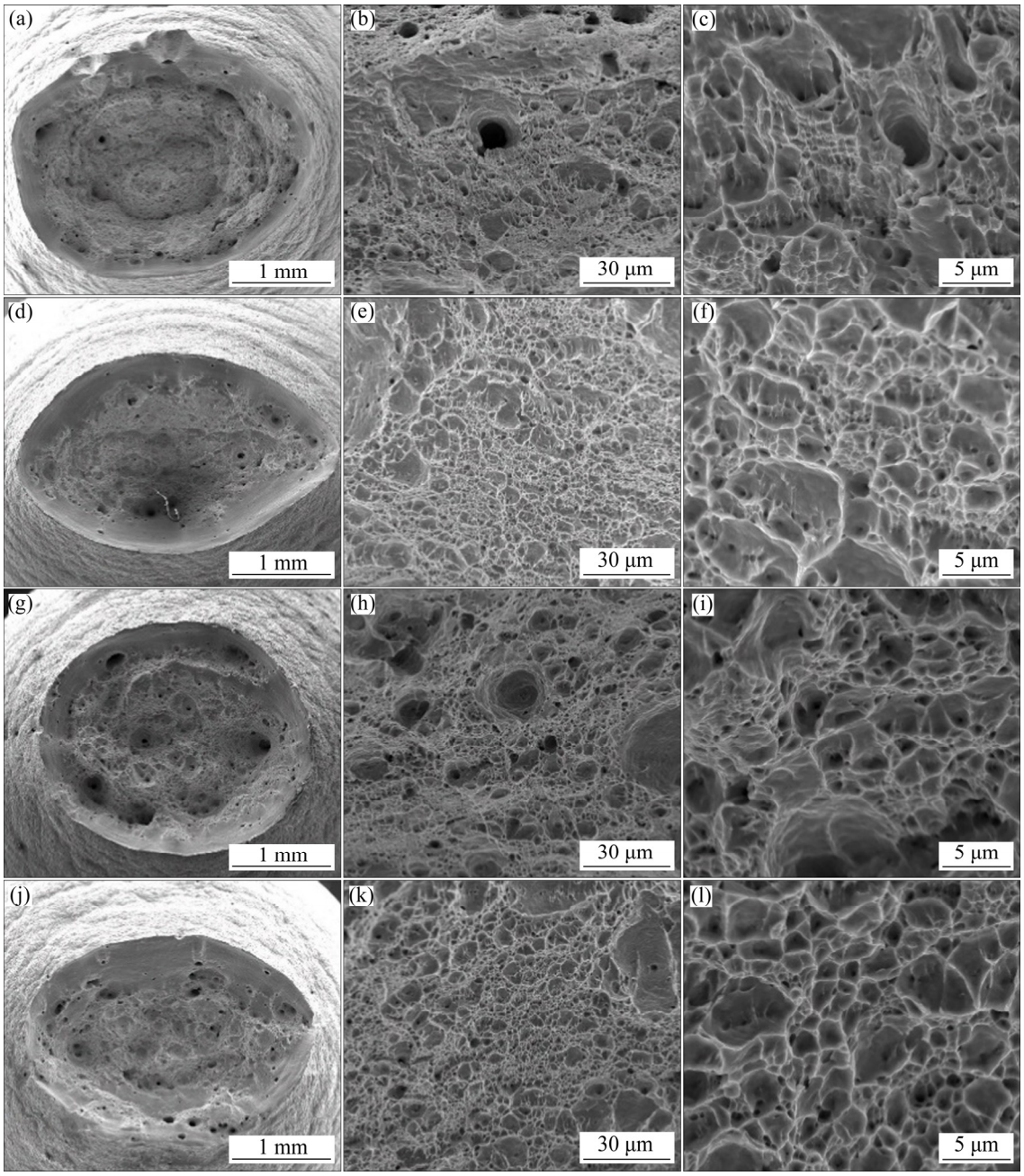


**Fig. 13** Morphologies for fracture surfaces of forged alloy (a−c) and alloy after annealing at 700 (d−f), 800 (g−i) and 900 °C (j−l) for 2 h

shaped, and some deep microvoids are approximately 10−15 μm, indicating that the alloy has excellent ductility. Additionally, a large number of fine dimples of only a few microns can be observed in the high magnification images, and the number of deep microvoids increases gradually with the increase of annealing temperature, which indicates that the ductility of the alloy is improved.

### 3.3 Electrical conductivity

After annealing at different temperatures for 2 h, the evolution of electrical conductivity of the alloy is shown in Fig. 14. It can be seen that the electrical conductivity of the forged alloy is 76% (IACS). After annealing at 600−700 °C, the electrical conductivity of the alloy is improved to a certain extent, and the peak value of 88% (IACS) is reached after annealing at 700 °C for 2 h. However, further increasing the annealing temperature leads to gradual decrease of electrical conductivity.

Generally, the electrical conductivity of deformed Cu alloy depends largely on the vacancies,

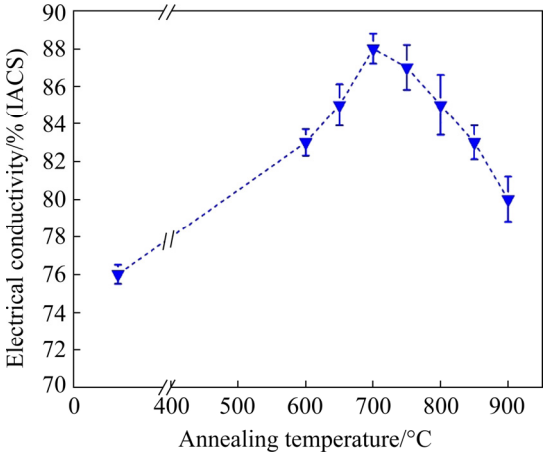


**Fig. 14** Effect of annealing temperature on electrical conductivity of Cu−0.15Zr alloy

dislocations, solutes and interfaces [35−37]. During the forging process, the alloy will inevitably produce vacancies and dislocations. When the alloy is annealed at 600−700 °C, the vacancy defects and dislocation density decrease with increasing the temperature. Additionally, the precipitation of Zr solutes from the matrix and the reduced number of interfaces by grain growth are conducive to weaken electronic scattering and improve the electrical conductivity of the alloy. However, after annealing at higher temperature (750−900 °C), the formation of a large number of nano-sized GB precipitates significantly increases the interface area, resulting in enhanced electron scattering and reduced electrical conductivity of the alloy. Additionally, the dissolution of large size granular $Cu_5Zr$ particles at high temperature increases the number of solute Zr atoms in the matrix, which leads to the increase of lattice distortion and is detrimental to the electrical conductivity. This result is also supported by similar observation from other researchers [38−40].

## 4 Conclusions

(1) The Zr-rich particles exhibit good thermal stability during elevated-temperature annealing. For the nano-sized $Cu_5Zr$ precipitates, no significant coarsening is observed even after annealing at 900 °C for 2 h, and the precipitates maintain a coherent relationship with the matrix. When the annealing temperature is higher than 700 °C, the large size $Cu_5Zr$ particles gradually dissolve into the matrix, accompanied by the formation of nano-sized GB precipitates, weakening the pinning effect of large size precipitates on GB migration and resulting in the grain growth.

(2) The Cu−0.15Zr alloy exhibits good comprehensive mechanical properties after high temperature annealing. When the annealing temperature is not higher than 750 °C, the UTS and YS drop slightly due to the continuous $Cu_5Zr$ precipitates and large size granular $Cu_5Zr$ particles increasing the microstructure stability. When the annealing temperature increases to 800 °C, the fraction of LAGBs, large size granular $Cu_5Zr$ particles and fine/equiaxed grains decrease sharply, resulting in a significant decrease in the strength of the alloy. Excellent ductility is obtained after annealing, and the fracture surface is dominated by ductile dimples.

(3) The electrical conductivity of Cu−0.15Zr alloy increases first and then decreases with the increase of annealing temperature, and reaches the peak of 88% (IACS) after annealing at 700 °C. The increase of conductivity is attributed to the decrease of defects scattering, GBs scattering and solute scattering. When the annealing temperature exceeds 750 °C, the increase in the number of the solute Zr atoms in the matrix and the formation of nano-sized GB precipitates lead to the decrease in the conductivity of the alloy.

## Acknowledgments

The authors are grateful for the financial supports from the Ministry of Science and Technology of China (No. 2017YFB0305701).

## References

[1] GAO L P, YANG X, ZHANG X F, ZHANG Y, SUN H L, LI N. Aging behavior and phase transformation of the Cu−0.2wt.%Zr−0.15wt.%Y alloy [J]. Vacuum, 2019, 159: 367−373. https://doi.org/10.1016/j.vacuum.2018.10.054.

[2] PURCEK G, YANAR H, SHANGINA D V, DEMIRTAS M, BOCHVAR N R, DOBATKIN S V. Influence of high pressure torsion-induced grain refinement and subsequent aging on tribological properties of Cu−Cr−Zr alloy [J]. Journal of Alloys and Compounds, 2018, 742: 325−333. https://doi.org/10.1016/j.jallcom.2018.01.303.

[3] ZHANG P C, SHI J F, YU Y S, SUN J C, LI T J. Effect of cryorolling on microstructure and property of high strength and high conductivity Cu−0.5wt.%Cr alloy [J]. Transactions of Nonferrous Metals Society of China, 2020, 30(9): 2472−2479. https://doi.org/10.1016/S1003-6326(20)65393-6.

[4] TIAN W, BI L M, MA F C, DU J D. Effect of Zr on as-cast microstructure and properties of Cu−Cr alloy [J]. Vacuum,

2018, 149: 238−247. https://doi.org/10.1016/j.vacuum.2017.12.011.

[5] SINGH R, LAWLEY A, FRIEDMAN S, MURTY Y V. Microstructure and properties of spray cast Cu−Zr alloys [J]. Materials Science and Engineering A, 1991, 145(2): 243−255. https://doi.org/10.1016/0921-5093(91)90254-K.

[6] BI L M, LIU P, CHEN X H, LIU X K, LI W, MA F C. Analysis of phase in Cu−15%Cr−0.24%Zr alloy [J]. Transactions of Nonferrous Metals Society of China, 2013, 23(5): 1342−1348. https://doi.org/10.1016/S1003-6326(13)62602-3.

[7] ZHAO J T, ZHANG J Y, CAO L F, WANG Y Q, ZHANG P, WU K, LIU G, SUN J. Zr alloying effect on the microstructure evolution and plastic deformation of nanostructured Cu thin films [J]. Acta Materialia, 2017, 132: 550−564. https://doi.org/10.1016/j.actamat.2017.05.007.

[8] NAKASHIMA K, MIYAMOTO K, KUNIMINE T, MONZEN R, MURAMATSU N. Precipitation behavior of Cu−Zr compounds in a Cu−0.13wt.%Zr alloy [J]. Journal of Alloys and Compounds, 2020, 816: 152650. https://doi.org/10.1016/j.jallcom.2019.152650.

[9] PENG L J, XIE H F, HUANG G J, LI Y F, YIN X Q, FENG X, MI X J, YANG Z. The phase transformation and its effects on properties of a Cu−0.12wt.%Zr alloy [J]. Materials Science and Engineering A, 2015, 633: 28−34. https://doi.org/10.1016/j.msea.2015.02.077.

[10] SHANGINA D V, BOCHVAR N R, MOROZOVA A I, BELYAKOV A N, KAIBYSHEV R O, DOBATKIN S V. Effect of chromium and zirconium content on structure, strength and electrical conductivity of Cu−Cr−Zr alloys after high pressure torsion [J]. Materials Letters, 2017, 199: 46−49. https://doi.org/10.1016/j.matlet.2017.04.039.

[11] GAGANOV A, FREUDENBERGER J, BOTCHAROVA E, SCHULTZ L. Effect of Zr additions on the microstructure, and the mechanical and electrical properties of Cu−7wt.%Ag alloys [J]. Materials Science and Engineering A, 2006, 437(2): 313−322. https://doi.org/10.1016/j.msea.2006.07.121.

[12] LIU J B, ZHANG L B, DONG A P, WANG L T, ZENG Y W, MENG L. Effects of Cr and Zr additions on the microstructure and properties of Cu−6wt.%Ag alloys [J]. Materials Science and Engineering A, 2012, 532: 331−338. https://doi.org/10.1016/j.msea.2011.10.099.

[13] SINGH J, JERMAN G, POORMAN R, BHAT B N, KURUVILLA A K. Mechanical properties and microstructural stability of wrought, laser, and electron beam glazed NARloy-Z alloy at elevated temperatures [J]. Journal of Materials Science, 1997, 32: 3891−3903. https://doi.org/10.1023/A:1018604513547.

[14] OKAMOTO H. Cu−Zr (copper−zirconium) [J]. Journal of Phase Equilibria and Diffusion, 2012, 33(5): 417−418. https://doi.org/10.1007/s11669-012-0077-1.

[15] WRIGHT R N, ANDERSON I E. Age-hardening behavior of dynamically consolidated rapidly solidified Cu−2%Zr powder [J]. Materials Science and Engineering A, 1989, 114: 167−172. https://doi.org/10.1016/0921-5093(89)90855-1.

[16] CORREIA J B, DAVIES H A, SELLARS C M. Strengthening in rapidly solidified age hardened Cu−Cr and Cu−Cr−Zr alloys [J]. Acta Materialia, 1997, 45(1): 177−190. https://doi.org/10.1016/S1359-6454(96)00142-5.

[17] ARNBERG L, BACKMARK U, BACKSTRÖM N, LANGE J. A new high strength, high conductivity Cu−0.5wt.%Zr alloy produced by rapid solidification technology [J]. Materials Science and Engineering, 1986, 83: 115−121. https://doi.org/10.1016/0025-5416(86)90178-3.

[18] CHEN F, ZHANG F, WANG J, ZHANG H L, TIAN R, ZHANG J, ZHANG Z, SUN F, WANG S W. Microstructure and optical properties of transparent aluminum oxynitride ceramics by hot isostatic pressing [J]. Scripta Materialia, 2014, 81: 20−23. https://doi.org/10.1016/j.scriptamat.2014.02.009.

[19] WANG M, ZHOU J X, YIN Y J, NAN H, XUE P J, TU Z X. Hot deformation behavior of the Ti6Al4V alloy prepared by powder hot isostatic pressing [J]. Journal of Alloys and Compounds, 2017, 721: 320−332. https://doi.org/10.1016/j.jallcom.2017.06.003.

[20] FU L H, HAN W, GONG K, BENGTSSON S, DONG C F, ZHAO L, TIAN Z L. Microstructure and tribological properties of $Cr_3C_2$/$Ni_3Al$ composite materials prepared by hot isostatic pressing (HIP) [J]. Materials and Design, 2017, 115: 203−212. https://doi.org/10.1016/j.matdes.2016.11.060.

[21] MORRIS D G, MORRIS M A, JOYE J C. High strength Cu−Zr alloys prepared by rapid solidification techniques [J]. Materials Science and Engineering A, 1992, 158(1): 111−117. https://doi.org/10.1016/0921-5093(92)90141-M.

[22] VINOFRADOV A, ISHIDA T, KITAGAWA K, KOPYLOV V I. Effect of strain path on structure and mechanical behavior of ultra-fine grain Cu−Cr alloy produced by equal-channel angular pressing [J]. Acta Materialia, 2005, 53(8): 2181−2192. https://doi.org/10.1016/j.actamat.2005.01.046.

[23] SHUKLA A K, SURESH KUMAR R, NARAYANA MURTY S V S, MONDAL K. Enhancement of high temperature ductility of hot-pressed Cu−Cr−Nb alloy by hot rolling [J]. Materials Science and Engineering A, 2013, 577: 36−42. https://doi.org/10.1016/j.msea.2013.04.043.

[24] SHUKLA A K, NARAYANA MURTY S V S, SURESH KUMAR R, MONDAL K. Effect of powder milling on mechanical properties of hot-pressed and hot-rolled Cu−Cr−Nb alloy [J]. Journal of Alloys and Compounds, 2013, 580: 427−434. https://doi.org/10.1016/j.jallcom.2013.06.118.

[25] LOU M Y W, GRANT N J. Identification of $Cu_5Zr$ phase in Cu−Zr alloys [J]. Metallurgical and Materials Transaction A, 1984, 15: 1491−1493. https://doi.org/10.1007/BF02648579.

[26] PAN Z Y, CHEN J B, LI J F. Microstructure and properties of rare earth-containing Cu−Cr−Zr alloy [J]. Transactions of Nonferrous Metals Society of China, 2015, 25(4): 1206−1214. https://doi.org/10.1016/S1003-6326(15)63717-7.

[27] ABDELJAWAD F, LU P, ARGIBAY N, CLARK B G, BOYCE B L, FOILES S M. Grain boundary segregation in immiscible nanocrystalline alloys [J]. Acta Materialia, 2017, 126: 528−539. https://doi.org/10.1016/j.actamat.2016.12.036.

[28] DONALDSON O K, HATTAR K, KAUB T, THOMPSON G B, TRELEWICZ J R. Solute stabilization of nanocrystalline tungsten against abnormal grain growth [J]. Journal of Materials Research, 2018, 33(1): 68−80. https://doi.org/10.

1557/jmr.2017.296.
[29] WANG T M, LI M Y, KANG H J, WANG W, ZOU C L, CHEN Z N. Effects of trace La additions on the microstructures and properties of nanoprecipitates strengthened Cu−Zr alloys [J]. Journal of Materials Research, 2015, 30(2): 248−256. https://doi.org/10.1557/jmr.2014.382.
[30] XU P, JIANG F, TANG Z Q, YAN N, JIANG J Y, XU X D, PENG Y Y. Coarsening of $Al_3Sc$ precipitates in Al−Mg−Sc alloys [J]. Journal of Alloys and Compounds, 2018, 781: 209−215. https://doi.org/10.1016/j.jallcom.2018.12.133.
[31] GAO Y H, CAO L F, KUANG J, ZHANG J Y, LIU G, SUN J. Dual effect of Cu on the $Al_3Sc$ nanoprecipitate coarsening [J]. Journal of Materials Science and Technology, 2020, 37: 38−45. https://doi.org/10.1016/j.jmst.2019.07.035.
[32] IWAMURA S, MIURA Y. Loss in coherency and coarsening behavior of $Al_3Sc$ precipitates [J]. Acta Materialia, 2004, 52(3): 591−600. https://doi.org/10.1016/j.actamat.2003.09.042.
[33] HE W J, CHEN X, LIU N, LUAN B F, YUAN G H, LIU Q. Cryo-rolling enhanced inhomogeneous deformation and recrystallization grain growth of a zirconium alloy [J]. Journal of Alloys and Compounds, 2017, 699: 160−169. https://doi.org/10.1016/j.jallcom.2016.12.300.
[34] GAO N, WANG S C, UBHI H S, STARINK M J. A comparison of grain size determination by light microscopy and EBSD analysis [J]. Journal of Materials Science, 2005, 40: 4971−4974. https://doi.org/10.1007/s10853-005-3867-6.
[35] WEI M Z, XU L J, SHI J, PAN G J, CAO Z H, MENG X K. Achieving high strength and high electrical conductivity in Ag/Cu multilayers [J]. Applied Physics Letters, 2015, 106(1): 011604. https://doi.org/10.1063/1.4905552.
[36] CAMACHO J M, OLIVA A I. Surface and grain boundary contributions in the electrical resistivity of metallic nanofilms [J]. Thin Solid Films, 2006, 515(4): 1881−1885. https://doi.org/10.1016/j.tsf.2006.07.024.
[37] DENG L P, HAN K, HARTWIG K T, SIEGRIST T M, DONG L Y, SUN Z Y, YANG X F, LIU Q. Hardness, electrical resistivity, and modeling of in situ Cu−Nb microcomposites [J]. Journal of Alloys and Compounds, 2014, 602: 331−338. https://doi.org/10.1016/j.jallcom.2014.03.021.
[38] BELOV N A, ALABIN A N, MATVEEVA I A, ESKIN D G. Effect of Zr additions and annealing temperature on electrical conductivity and hardness of hot rolled Al sheets [J]. Transactions of Nonferrous Metals Society of China, 2015, 25(9): 2817−2826. https://doi.org/10.1016/S1003-6326(15)63907-3.
[39] ZHANG J Y, MA M Y, SHEN F H, YI D Q, WANG B. Influence of deformation and annealing on electrical conductivity, mechanical properties and texture of Al−Mg−Si alloy cables [J]. Materials Science and Engineering A, 2018, 710: 27−37. https://doi.org/10.1016/j.msea.2017.10.065.
[40] WU Z W, LIU J J, CHEN Y, MENG L. Microstructure, mechanical properties and electrical conductivity of Cu−12wt.%Fe microcomposite annealed at different temperatures [J]. Journal of Alloys and Compounds, 2009, 467(1−2): 213−218. https://doi.org/10.1016/j.jallcom.2007.12.020.

# 高温退火对 Cu−0.15Zr 合金显微组织和性能的影响

张子辰[1]，王日初[1,2]，彭超群[1]，冯 艳[1,2]，王小锋[1,2]，吴 翔[3]，蔡志勇[1,2]

1. 中南大学 材料科学与工程学院，长沙 410083；
2. 中南大学 电子封装与先进功能材料湖南省重点实验室，长沙 410083；
3. 长沙理工大学 材料科学与工程学院，长沙 410114

**摘 要**：采用快速凝固与热锻相结合的方法，制备组织均匀、晶粒细小的 Cu−0.15Zr(质量分数，%)合金，研究高温退火过程中合金显微组织演变、力学性能和电导率。该合金表现出良好的热稳定性，即使在 700 °C 退火 2 h 后，合金强度仅轻微下降。退火过程中纳米级连续分布的 $Cu_5Zr$ 析出相对位错运动起到钉扎作用，从而使基体强化，同时，尺寸较大的颗粒状 $Cu_5Zr$ 析出相通过钉扎晶界阻碍晶粒长大。在 700 °C 退火 2 h 后，由于空位、位错、晶界以及基体中溶质 Zr 原子减少，合金电导率达到峰值 88% (IACS)。

**关键词**：Cu−Zr 合金；快速凝固；退火；显微组织；抗拉强度；电导率

**(Edited by Bing YANG)**